16th International Conference on Greenhouse Gas Control Technologies, GHGT-16

23rd -27th October 2022, Lyon, France

Deep Learning Accelerated Inverse Modeling and Forecasting for Large-Scale Geologic CO_2 Sequestration

Bailian Chen[a,*], Bicheng Yan[a,b], Qinjun Kang[a], Dylan Harp[a,c], Rajesh Pawar[a]

[a]*Earth and Environmental Sciences Division, Los Alamos National Laboratory, NM 87545, USA*
[b]*Physical Science and Engineering Division, King Abdullah University of Science and Technology, Thuwal 23955, Saudi Arabia*
[c]*The Freshwater Trust, OR 97205, USA*

Abstract

Traditional physics-simulation based approaches for inverse modeling and forecasting in geologic CO_2 sequestration (GCS) are very time consuming. A single inverse modeling and forecasting process using traditional physics-based approaches (e.g., Ensemble Smoother with Multiple Data Assimilation or Ensemble Kalman Filter) may take a few weeks for a large-scale CO_2 storage model (~million grid cells) without leveraging any high-performance computing. To speed up this process, researchers from the U.S. Department of Energy's SMART Initiative (https://edx.netl.doe.gov/smart/) have developed multiple approaches that employ machine learning methods to integrate monitoring data into subsurface forecasts more rapidly than current physics-based inverse modeling workflows allow. These updated forecasts with the updated models from the inverse modeling (history matching) process will be used to provide site operators with decision support by generating real-time performance metrics of CO_2 storage (e.g., CO_2 plume and pressure area of review). Here, we present one such machine learning accelerated workflow that can speed up the inverse modeling and forecasting process by three orders of magnitude. First, we developed a deep learning (DL) model to predict the pressure/saturation evolution in large-scale storage reservoirs. A feature coarsening technique was applied to extract the most representative information and perform the training and prediction at the coarse scale, and to further recover the resolution at the fine scale by 2D piecewise cubic interpolation. The accuracy of the feature coarsening-based DL model is validated with a reservoir model (~1.34 million grid cells) built upon a Clastic Shelf storage site. The overall mean relative error between the ground truth and the predictions from DL workflow is no more than 0.2%. Thereafter, the feature coarsening based deep learning model was utilized as forward model in the inverse modeling process where a classical data assimilation approach, ES-MDA-GEO, was applied. The efficiency and effectiveness of the proposed deep learning assisted workflow for large-scale inverse modeling and forecasting was demonstrated with the Clastic Shelf storage model.

Keywords: CCS; Geologic CO_2 Sequestration; Inverse Modeling; Rapid Forecasting; Deep Learning; Feature Coarsening Technique

* Corresponding author. Tel.: +1-505-667-1926, *E-mail address:* bailianchen@lanl.gov

1. Introduction

Fluid flow in porous media drives the overall performance of many geologic CO_2 storage (GCS) and energy extraction processes. In physics-based simulations, the governing equations used to describe fluid flow in porous media can be accurately discretized by traditional numerical methods and thus the temporal-spatial evolution of state variables (e.g., pressure and saturation) in the porous media can be accurately predicted. The main drawback of this approach is the high computational expense, which is associated with the scale of the geological model and the nonlinearity due to heterogeneities, complex fluid thermodynamics, and coupled physics processes.

As researchers have demonstrated deep learning's (DL) superior capability to process high dimensional data [1] and approximate various continuous functions [2], many recent research studies focus on enhancing the capability to predict the evolution of state variables in porous media with DL. A family of physics-informed neural network (PINN) models impose physics governing equations to regularize the loss function during the training process through automatic differentiation [3, 4]. These approaches ensure that the neural networks are consistent with the physics governing fluid flow in porous media. While PINN is suitable for predicting processes governed by physics with medium complexity, its use may become computationally expensive to solve problems with large scale and high nonlinearity. Alternatively, image-based approaches have also been investigated to predict fluid flow in porous media, and mainly leverage convolutional neural networks (CNN) to approximate the nonlinear relationship between geological maps and flow maps in fluid flow in porous media [5, 6]. With sparse connectivity between input and output, image-based approaches tend to be more appropriate to deal with medium-scale heterogeneous porous media. However, for capturing heterogeneity with high resolution, the scale of a realistic geological model can easily reach millions of grid cells, which is extremely challenging for existing DL methodologies to digest the data for temporal and spatial regression tasks. So far there is little work to evaluate the training efficiency and predictive accuracy of the evolution of state variables in such large heterogeneous geological models.

Here, we describe a DL workflow to predict the evolution of pressure as fluid flows in large-scale 3D geological models. This workflow falls into the category of image-based approaches, as it takes full advantage of the spatial topology predictive capability [7, 8] of CNN, specifically Fourier Neural Operator (FNO) [9]. In this work, we apply feature coarsening technique to extract the most representative information from the input maps and perform the training and prediction of FNO at the coarse space [10]. This can significantly decrease the memory consumption of the training data and computational cost for training, and thus makes DL more affordable for large scale geological models. Based on the hypothesis of pressure/saturation continuity, we further recover the resolution of predicted pressure/saturation fields to the original fine scale through 2D piecewise cubic interpolation approach. To validate the performance, we apply the DL workflow that is trained from physics-based simulation data to predict the pressure/saturation evolution in a field-scale 3D heterogeneous geological CO_2 storage reservoir, and provide comprehensive analysis to assess the memory efficiency, training efficiency and predictive accuracy of the DL workflow.

In the last decade, ensemble-based methods have been widely used for history matching of sub-surface flow problems in both hydrologic applications and the petroleum industry. Among the ensemble-based methods, the ensemble Kalman filter (EnKF) is the most popular for history matching applications [11,12]. Emerick and Reynolds [13] proposed a new data assimilation approach, i.e., Ensemble Smoother with Multiple Data Assimilation (ES-MDA) and demonstrated the superiority of ES-MDA over EnKF for data assimilation. The main drawback of ES-MDA is that the total number of data assimilation steps and the inflation factors for each assimilation iteration must be specified before starting data assimilation processes. Recently, a more practical and efficient version of this approach called ES-MDA with geometric inflation factors (ES-MDA-GEO) was proposed by Rafiee and Reynolds [14]. This method allows the user to specify a priori the total number of data assimilation steps which is determined based on the allowable computational resources, while at the same time providing sufficient damping of changes in the reservoir model realizations. This recently developed algorithm, ES-MDA-GEO, is implemented in this study for assimilating monitoring data collected during GCS projects. Traditional physics-simulation based approaches for inverse modeling and forecasting in geologic CO_2 sequestration (GCS) are very time consuming [15].

The objective of this work is to develop a workflow that employs DL methods to integrate monitoring data into subsurface forecasts more rapidly than current physics-based history matching workflows allow. The feature coarsening based DL proxy model developed can be used to predict the pressure/saturation evolution in large-scale

storage reservoir. We apply this DL proxy model as forward model in the history matching process where a classical data assimilation approach, ES-MDA-GEO, is used. The proposed workflow is demonstrated with a reservoir model built upon a Clastic Shelf storage site for history matching and forecasting under uncertainty.

This paper is organized as follows: Section 2 presents the proposed DL accelerated workflow for history matching and forecasting. The reservoir model description, DL model training and results are presented in Section 3. The major observations are summarized in Section 4.

2. Methodology

The proposed workflow for history matching and forecasting is shown in Fig. 1. This workflow includes two major components: History Matching Engine and Forward Modeling Engine. The history matching engine is driven by the most advanced version of ES-MDA, i.e., ES-MDA-GEO, while the forward modeling engine is based on FNO deep learning model (an image-based approach) [9]. As demonstrated in our previous work [10], assembly of the 2D feature images as a feature array will consume large quantities of memory, which can potentially lead to memory allocation issue and low training efficiency. Therefore, we plan to coarsen the image size to a certain level before proceeding to the training process. In this work, the feature images are coarsened by selecting spatial points with a constant stride, which is defined as an increment value added to the preceding spatial point in order to generate the next spatial point, while we always keep the most representative information, such as high permeability and porosity zones and injection well locations. Correspondingly, the output images (e.g., pressure) are also processed in the same way. The accuracy and efficiency of feature coarsening-based DL proxy model has been demonstrated in our previous work [10]. In this paper, we mainly focus on the demonstration of the proposed DL accelerated workflow for history matching (inversing modeling) and forecasting in GCS.

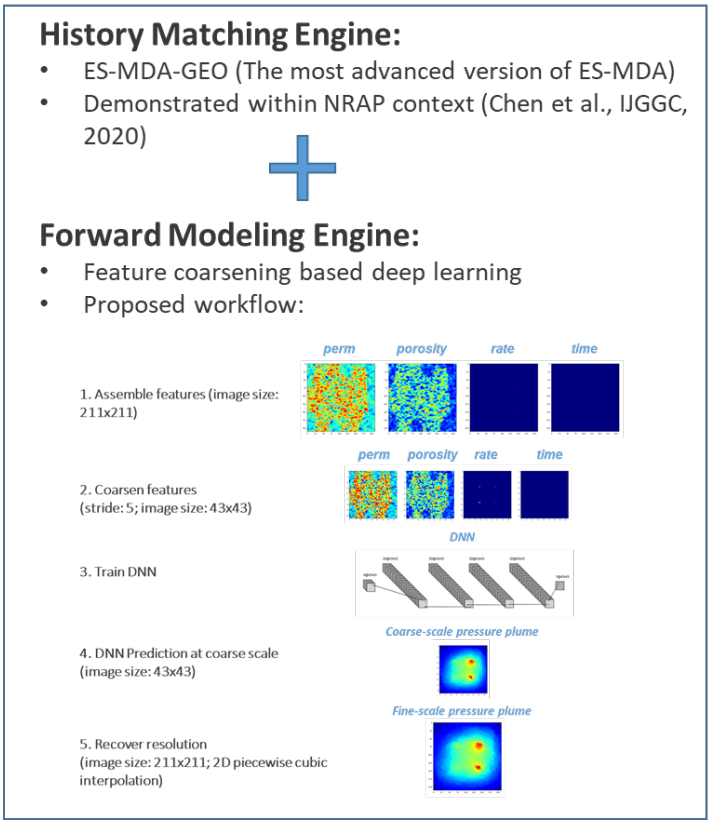

Fig. 1. The proposed workflow for history matching and forecasting.

3. Results

3.1. Reservoir model description and DL model accuracy

A 3D heterogeneous reservoir model with 211 by 211 by 30 grid cells in the x, y and z directions respectively is used. The total number of grid cells is ~1.3 million. The grid dimension is 500 ft by 500 ft by 10 ft in the x, y and z directions, respectively, and cell size is uniform throughout the domain. The schematic of the reservoir model is depicted in Fig. 2. There are 2 layers (layers 1 and 2) of "caprock" to seal CO_2 at the top, and 28 layers (layer 3 to 30) of "storage zone" to store CO_2. There are 4 CO_2 injection wells perforating all the 28 layers in the "storage zone". Two million tons of CO_2 was injected at a constant rate for 10 years with 32 timesteps. The permeability and porosity fields are correlated and assumed to be spatially heterogeneous and uncertain. 100 equiprobable realizations of permeability and porosity fields are generated following the same geological facies model. Fig. 3 presents 3 examples of the permeability realizations of the storage zone and the corresponding porosity realizations. In each example the shapes of the high permeability and porosity zones are quite similar, but the magnitudes of permeability and porosity in these zones vary.

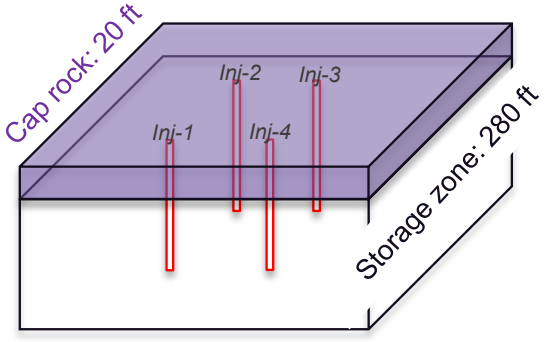

Fig. 2. Schematic of the reservoir model for geological CO_2 storage.

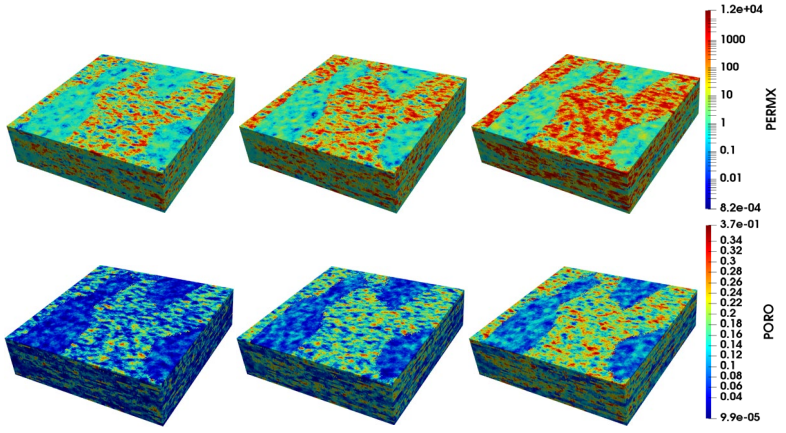

Fig. 3. Realizations of P25, P50, and P75 (left to right) for permeability (top) and porosity (bottom) of the reservoir model.

100 simulations were performed on each of the model with the commercial reservoir simulation, GEM from CMG (CMG, 2020) to generate training data for the DL workflow. The ensemble of realizations is split based on the permeability and porosity realizations where we choose 90 simulation runs for training, 5 runs for validation and 5 runs for testing. In Fig. 4, we present a representative example of the pressure fields at early and late times in the top (layer 3), middle (layer 16) and bottom (layer 30) layers in the "storage zone" for predictions of the DL workflow with FNO (stride = 3), and compare them with the ground truth from reservoir simulation. At the early period (1 year)

the pressure plumes grow surrounding the 4 injection wells and the plume becomes larger with increasing depth (larger layer number) because of gravity. These details are captured by the predictions from our DL workflow (mean absolute error 2.826 psia and mean relative error 0.149%), and there are only small errors in the injection well locations. At the end of the CO_2 injection period (10 years) the pressure plume reaches its maximum size with the pressure error increasing slightly (mean absolute error 3.906 psia and mean relative error 0.202%). Besides, we observe that the DL workflow can generally predict smooth pressure field and delineates the irregular pressure plume shape driven by permeability and porosity heterogeneity quite well, especially for larger plume sizes. More details about the DL model accuracy can be found in our previous work [10].

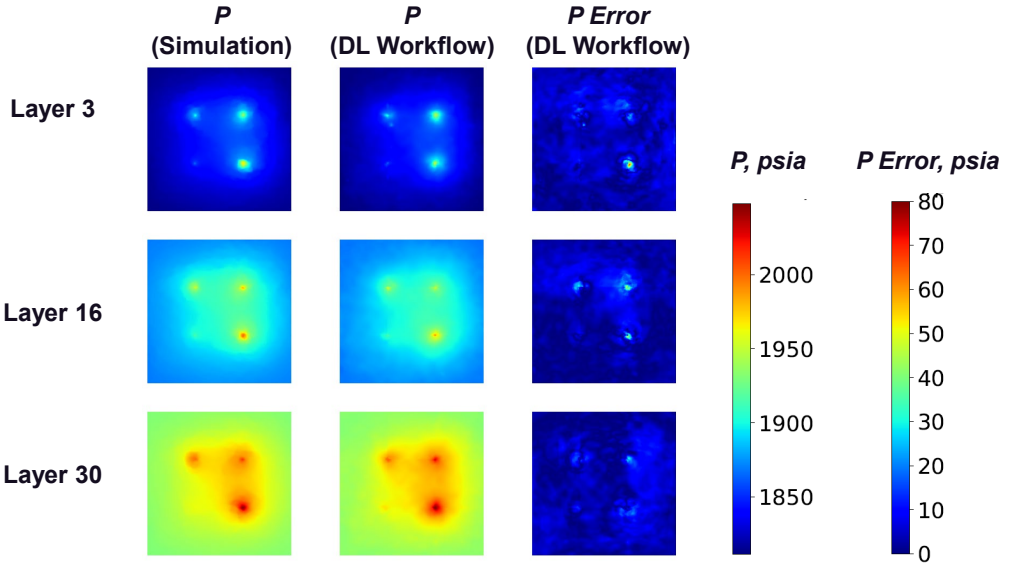

(a) Pressure after 1 year injection. Mean absolute error: 2.826 psia, mean relative error: 0.149%.

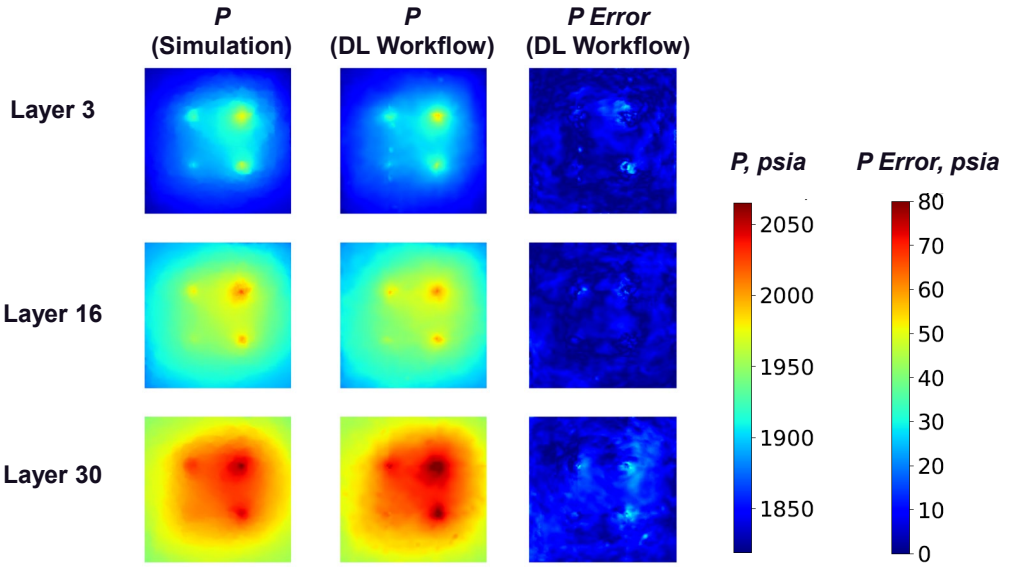

(b) Pressure after 10-year injection. Mean absolute error: 3.906 psia, mean relative error: 0.202%.

Fig. 4. Pressure prediction by the DL workflow with FNO (stride = 3).

3.2. History matching and forecasting

Fig. 5 show the log permeability of layer 3 and the well locations for injection wells, monitoring wells and testing (legacy) wells. Given that the CO_2 saturation plume is extremely small, we only consider the pressures data collected from injection wells and monitoring wells as observational data. One pressure data becomes available as time elapses by a month up to 2 years and a year to 10 years (i.e., one pressure data per month in the first two years and one pressure data per year in the remaining 8 years). The model realization P50-1 is chosen as the ground truth model, and the observational data are generated from this model realization. The remaining 99 modes are considered as prior models in the history matching process. Two scenarios are considered: a scenario with 4 injectors only (case 1) and a scenario with 4 injectors and 2 monitoring wells (case 2).

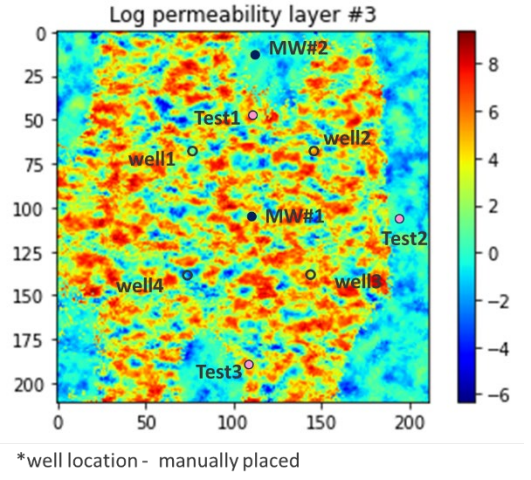

Fig. 5. Log permeability distribution of layer 3, and the well locations for four injection wells (well1, well 2, well3 and well4), 2 monitoring wells (MW#1 and MW#2) and 3 testing wells (Test1, Test2 and Test3).

Fig. 6 shows the results of history matching 1.5 years pressure data and forecasting remaining 8.5 years for the case with 4 injectors only (case 1) and the case with 4 injectors and 2 monitoring wells (case 2). As we can see, all the history data (in red circles) are well matched with the predictions (in dark blue curves) from the posterior (updated) models. The uncertainty in the pressure predictions based on the updated models from year 1.5 to year 10 is significantly reduced compared to the uncertainty in the predictions (in light blue curves) based on the prior models. In addition, the uncertainty in the predictions of pressure in the four injection wells in case 1 is slightly smaller (i.e., tighter curves) than the uncertainty in the predictions in the four injectors (e.g., injection well I3) in case 2. This is mainly because the data collection from two monitoring wells in case 2 helps reducing uncertainty in predictions.

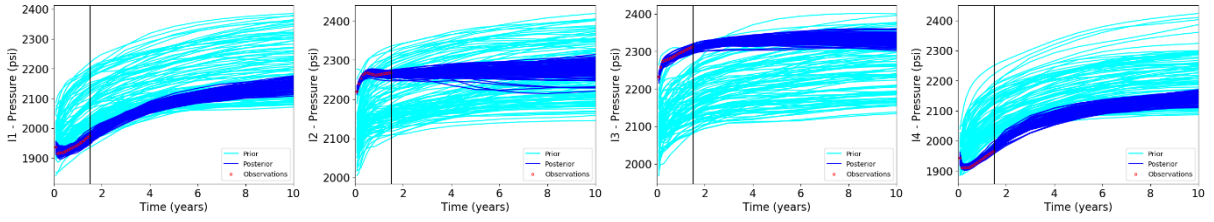

(a) Case 1: 4 injectors only

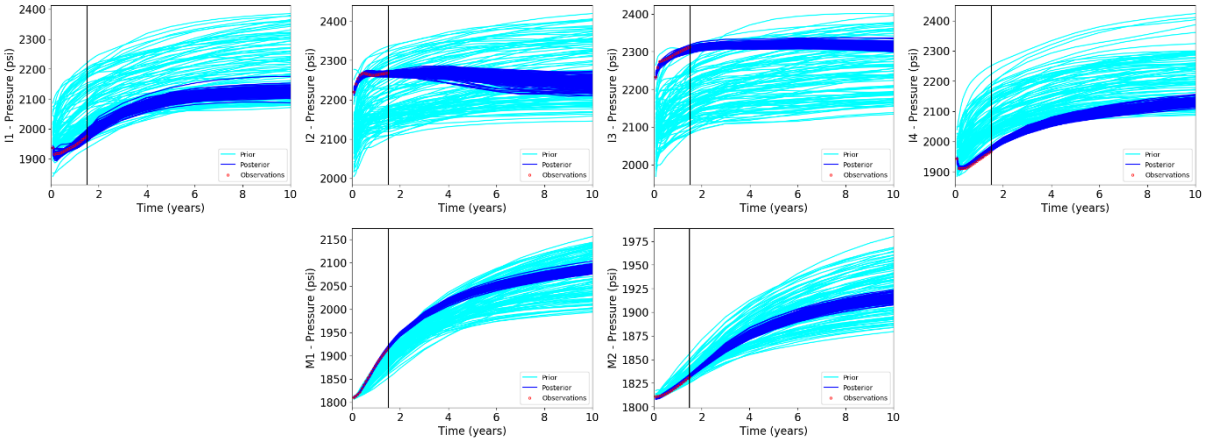

(b) Case 2: 4 injectors + 2 monitoring wells

Fig. 6. History matching 1.5 years pressure data and forecasting pressures for the remaining 8.5 years. Light blue curves correspond to the predictions from 99 prior models, while dark blue curves correspond to the predictions based on the posterior (updated) models.

3.3. Forecasts at the testing (legacy) wells

The pressure forecasts in the three legacy wells under two different cases are displayed in Fig. 7. Overall, the uncertainty in the forecasts based on the updated models is significantly smaller than that based on the prior models. We can also observe that the case with 4 injectors and 2 monitoring wells can reduce more uncertainty in the predictions of pressure in legacy wells compared to the case with only 4 injectors. This is mainly because more data are collected for the scenario with 4 injectors and 2 monitoring wells, and more history data lead to more uncertainty reduction.

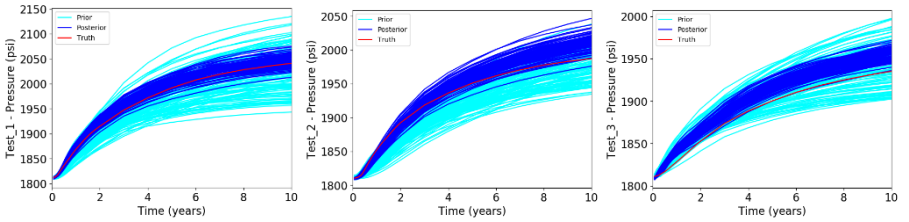

(a) Case 1: 4 injectors only

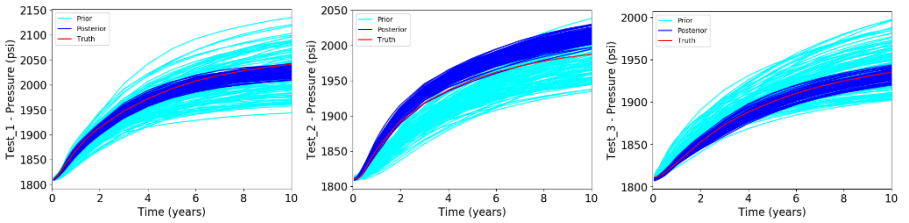

(b) Case 2: 4 injectors + 2 monitoring wells

Fig. 7. Pressure forecasts at the legacy wells based on the prior and the updated models with 1.5 years history data.

3.4. Reservoir pressure plume area of review (delta P > 20 PSI)

The pressure plume area of review (AOR) was calculated based on the threshold of 20 psi. The boxplots of pressure AOR based on prior models and updated models (with 1.5 years history data) at the end of year 10 are shown in Fig. 8. From this figure, we can observe that the uncertainty in the predictions of pressure plume AOR based on posterior (updated) models has been significantly reduced compared to the predictions based on the prior models. In addition, the uncertainty in the posterior predictions under the case with 4 injectors is larger than that under the case with 4 injectors and 2 monitoring wells, i.e., the band width of the boxplot for posterior predictions under case 2 is smaller than case 2. It is also interesting to see that though the posterior predictions in case 2 are all smaller than the ground truth (in red line), but they are not significantly off from the ground truth. In the reality, we never know the ground truth. We add the ground truth here just for reference.

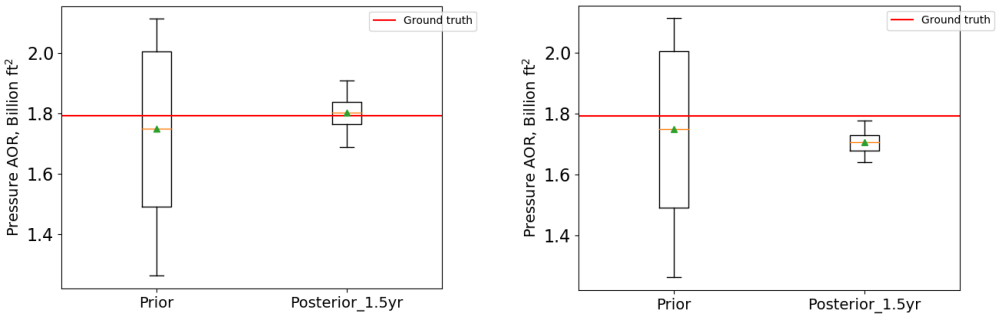

(a) Case 1: 4 injectors only (b) Case 2: 4 injectors + 2 monitoring wells

Fig. 8. Pressure plume area of review (AOR) at the end of year 10 for two different cases.

3.5. Model updating

Fig. 9 shows the updated permeability fields for the third layer of reservoir model after matching 1.5 years history data. As we can see, the posterior models are more similar to the ground truth model compared to the prior models, especially for the realizations of R11 and R31. The updated models in case 2 (4 injectors and 2 monitoring wells) is much closer to the ground truth model than the updated models in case 1.

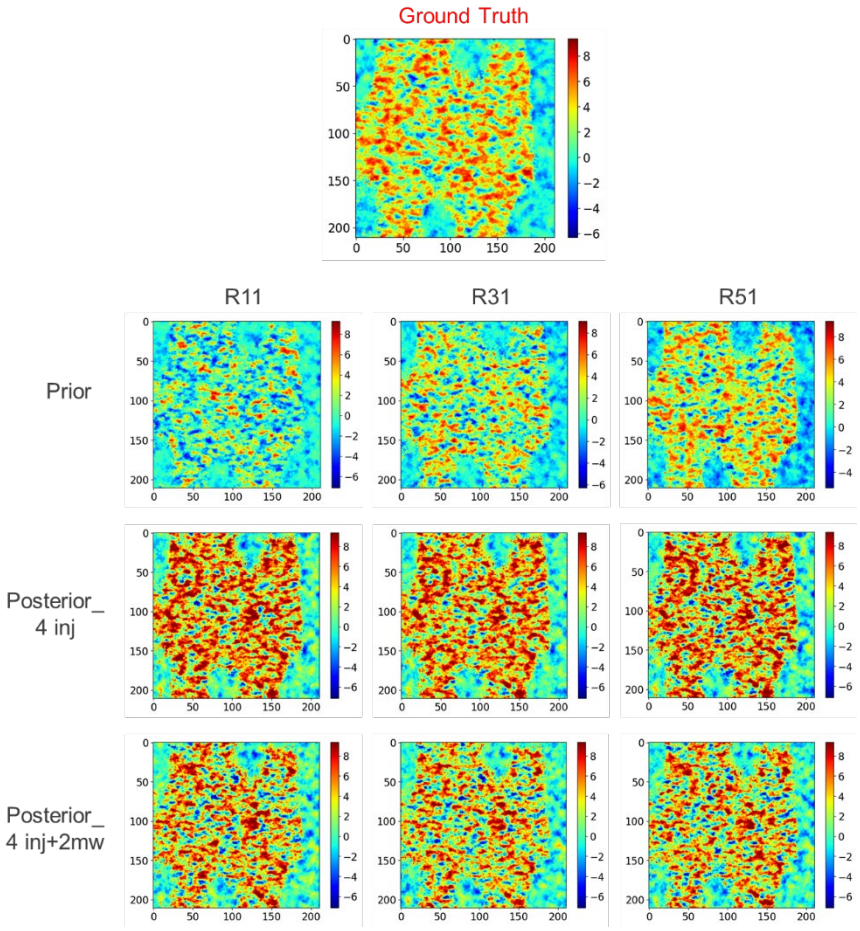

Fig. 9. The ground truth log permeability field, log permeability fields for prior models and posterior models for three model realizations, R11, R31 and R51.

3.6. Impact of monitoring duration

In this study, we also investigate the impact of the monitoring durations. Here, different monitoring durations, i.e., 1.5 years, 2 years, 5 years and 10 years, are considered. As we can see from Fig. 10, with the increase of the monitoring durations, the uncertainty in the predictions of pressures in the legacy well decreases. Unfortunately, we only have 10 years history data, we cannot investigate when the trend of uncertainty reduction will stop, i.e., no further VOI with additional data collection. In addition, the data frequency after 2 years is once per year (i.e., one pressure data per year). It is unclear whether higher frequency of data collection will result in more uncertainty reduction. It is important to note that we also observe the uncertainty reduction in other quantities (e.g., pressure plume AOR) with the increase of monitoring durations, which are not shown here.

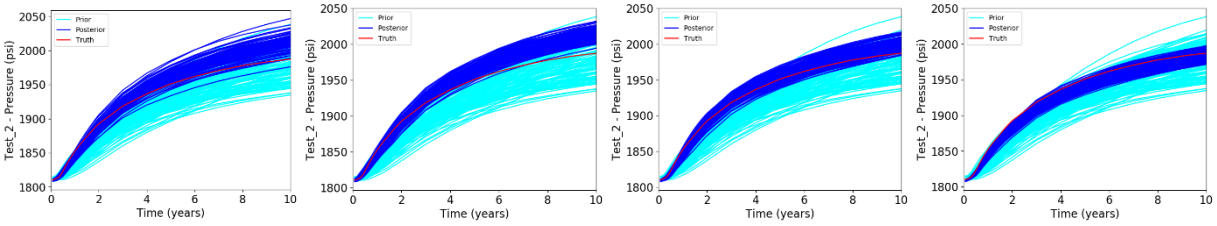

(a) 1.5 years (b) 2 years (c) 5 years (d) 10 years

Fig. 10. Pressure predictions in the legacy wells over monitoring duration; case 1.

Conclusions

In this study, we have demonstrated that the proposed workflow based on classical history matching approach ES-MDA-GEO combined with FNO deep learning model leveraging feature coarsening technique is suitable and efficient for near real-time history matching and forecasting. We observed that the computational time for running the DL accelerated workflow for history matching and forecasting based on the Clastic Shelf model is three orders of magnitude faster than traditional history matching approach (i.e., physics simulation based ES-MDA-GEO history matching process). In the future work, we will consider more observational data, including CO_2 saturation and temperature measurements from monitoring wells and spatial data such as saturation images interpreted from 3D seismic survey, in our history matching process.

Acknowledgements

This work was supported by the US Department of Energy through the Los Alamos National Laboratory. Los Alamos National Laboratory is operated by Triad National Security, LLC, for the National Nuclear Security Administration of U.S. Department of Energy (Contract No. 89233218CNA000001). The authors acknowledge the financial support by US DOE's Fossil Energy Program Office through the project, Science-informed Machine Learning to Accelerate Real Time (SMART) Decisions in Subsurface Applications. Funding for SMART is managed by the National Energy Technology Laboratory (NETL).

References

[1] Georgious, T., Liu, Y., Chen, W., Lew, M. 2020. A Survey of Traditional and Deep Learning-based Feature Descriptors for High Dimensional Data in Computer Vision. International Journal of Multimedia Information Retrieval 9: 135: 170.

[2] Csaji, B.C. 2001. Approximation with Artificial Neural Networks. Faculty of Sciences, Etvs Lornd University, 24.

[3] Fuks, O., Tchelepi, H.A., 2020. Limitations of physics informed machine learning for nonlinear two-phase transport in porous media. Journal of Machine Learning for Modeling and Computing.

[4] Harp, D.R., O'Malley, D., Yan, B., Pawar, R. 2021. On the feasibility of using physics-informed machine learning for underground reservoir pressure management. Expert Systems With Applications 178, 115006.

[5] Zhong, Z., Sun, A.Y., Jeong, H. 2019. Predicting CO_2 Plume Migration in Heterogeneous Formations Using Conditional Deep Convolutional Generative Adversarial Networks. Water Resources Research, 55: 5830-5851.

[6] Tang, M., Liu, Y., Durlofsky, L.J. 2020. A Deep-Learning-based Surrogate Model for Data Assimilation in Dynamic Subsurface Flow Problems. Journal of Computational Physics, 413 (2020) 109656.

[7] Hughes, L.H., Schmitt, M., Mou, L., Wang, Y., Zhu, X. 2018. Identifying Corresponding Patches in SAR and Optical Images with a Pseudo-Siamese CNN. IEEE Geoscience and Remote Sensing Letters, Vol. 15, Issue: 5.

[8] Huang, L., Chen, Y. 2020. Dual-Path Siamese CNN for Hyperspectral Image Classification With Limited Training Samples. IEEE Geoscience and Remote Sensing Letters, Vol. 18, Issue: 3.

[9] Li, Z., Kovachki, N., Azizzadenesheli, K., Liu, B., Bhattacharya, K., Stuart, A., Anandkumar, A. 2020. Fourier Neural Operator for Parametric Partial Differential Equations. arXiv:2010.08895.

[10] Yan, B., Harp, D. R., Chen, B., & Pawar, R. J. 2021. Improving Deep Learning Performance for Predicting Large-Scale Porous-Media Flow through Feature Coarsening. *arXiv preprint arXiv:2105.03752*.
[11] Evensen, G. (2009). Data assimilation: the ensemble Kalman filter, Springer Science & Business Media.
[12] Chen, Y. and D. S. Oliver (2010). Cross-covariances and localization for EnKF in multiphase flow data assimilation. Computational Geosciences 14(4): 579-601.
[13] Emerick, A. A. and A. C. Reynolds (2013). Ensemble smoother with multiple data assimilation. Computers & Geosciences 55: 3-15.
[14] Rafiee, J. and A. C. Reynolds (2017). Theoretical and efficient practical procedures for the generation of inflation factors for ES-MDA. Inverse Problems 33: 115003.
[15] Chen, B., Harp, D. R., Lu, Z., & Pawar, R. J. (2020). Reducing uncertainty in geologic CO_2 sequestration risk assessment by assimilating monitoring data. International Journal of Greenhouse Gas Control, 94, 102926.